Vav3 Is Involved in GABAergic Axon Guidance Events Important for the Proper Function of Brainstem Neurons Controlling Cardiovascular, Respiratory, and Renal Parameters

Vincent Sauzeau,* José A. C. Horta-Junior,† Adelaida S. Riolobos,†‡ Gloria Fernández,§ María A. Sevilla,*‡ Dolores E. López,† María J. Montero,*‡ Beatriz Rico,§ and Xosé R. Bustelo*

*Centro de Investigación del Cáncer, CSIC-Salamanca University, †Instituto de Neurociencias de Castilla y León and ‡Departamento de Fisiología y Farmacología, Salamanca University, 37007 Salamanca, Spain; and §Instituto de Neurociencias, CSIC-Miguel Hernández University, 03550 Sant Joan d'Alacant, Spain

Vav3 is a phosphorylation-dependent activator of Rho/Rac GTPases that has been implicated in hematopoietic, bone, cerebellar, and cardiovascular roles. Consistent with the latter function, Vav3-deficient mice develop hypertension, tachycardia, and renocardiovascular dysfunctions. The cause of those defects remains unknown as yet. Here, we show that Vav3 is expressed in GABAegic neurons of the ventrolateral medulla (VLM), a brainstem area that modulates respiratory rates and, via sympathetic efferents, a large number of physiological circuits controlling blood pressure. On Vav3 loss, GABAergic cells of the caudal VLM cannot innervate properly their postsynaptic targets in the rostral VLM, leading to reduced GABAergic transmission between these two areas. This results in an abnormal regulation of catecholamine blood levels and in improper control of blood pressure and respiration rates to GABAergic signals. By contrast, the reaction of the rostral VLM to excitatory signals is not impaired. Consistent with those observations, we also demonstrate that Vav3 plays important roles in axon branching and growth cone morphology in primary GABAergic cells. Our study discloses an essential and nonredundant role for this Vav family member in axon guidance events in brainstem neurons that control blood pressure and respiratory rates.

INTRODUCTION

Vav3 is one of the three members of the Vav family present in vertebrate species (Bustelo, 2000; Bustelo and Couceiro, 2008). The main known function of these proteins is to act as GDP/GTP exchange factors for Rho/Rac GTPases, an activity that allows the rapid transition of Rho/Rac proteins from the inactive (GDP-bound) to the active (GTP-bound) state (Bustelo, 2000; Turner and Billadeau, 2002). Because the activity of Vav proteins is regulated by direct phosphorylation on tyrosine residues (Bustelo, 2000; Turner and Billadeau, 2002), the members of this family are crucial for connecting stimulated receptors with intrinsic or associated tyrosine kinase activity to Rho/Rac proteins and, thereby, to assemble downstream pathways involved in cytoskeletal change, cell cycle transitions, gene expression, and cell type–specific biological processes such as immune responses to

antigens, phagocytosis, production of reactive oxygen species, neuritogenesis, or axon guidance (Bustelo, 2000; Bustelo and Couceiro, 2008). Adaptor-like functions for Vav proteins have been also described during the signaling of antigen receptors (Bustelo, 2001; Saveliev *et al.*, 2009).

Vav3 plays overlapping roles with other Vav family members in the hematopoietic system (Fujikawa *et al.*, 2003; Cella *et al.*, 2004; Gakidis *et al.*, 2004; Pearce *et al.*, 2004; Hall *et al.*, 2006; Miletic *et al.*, 2007; Pearce *et al.*, 2007), axon guidance of neuronal subsets (Cowan *et al.*, 2005), and angiogenesis (Hunter *et al.*, 2006). Recent data also indicate that Vav3 exerts specific signaling tasks on its own, including the proper maturation and signaling of osteoclasts (Faccio *et al.*, 2005), timely cerebellar development (Quevedo *et al.*, 2010), and the regulation of cardiovascular parameters (Sauzeau *et al.*, 2006; Sauzeau *et al.*, 2007). As a consequence of the latter function, $Vav3^{-/-}$ mice develop tachycardia, a renin/angiotensin II (AngII)–dependent hypertension, cardiovascular remodeling, and renal dysfunctions (Sauzeau *et al.*, 2006). This phenotype resembles that found in patients with hyperkinetic hemodynamics and borderline hypertension (Julius and Nesbitt, 1996). The cause of the hypertensive phenotype of $Vav3^{-/-}$ mice is as yet unknown. However, experimental evidence suggest that it may be caused by the chronic hyperactivation of the sympathetic nervous system (SNS), because Vav3-deficient mice have tachycardia and contain abnormal high levels of catecholamines in their plasma (Sauzeau *et al.*, 2006). These defects, unlike other

cardiovascular problems that are detected later on, are already present in new born animals (Sauzeau *et al.*, 2006). Consistent with an implication of the SNS, the development of the hypertension, the tachycardia, and the rest of reno-cardiovascular phenotypes found in $Vav3^{-/-}$ mice is blocked by treatments with propranolol, a β-adrenergic antagonist commonly used in antihypertensive therapies (Sauzeau *et al.*, 2006). To understand the biological problems associated with this cardiovascular phenotype, we analyzed further the physiological and biological dysfunctions present in Vav3-deficient mice. Herein, we show that these animals have axon guidance defects in a subset of GABAergic cells of the VLM, a key brainstem center for the modulation of respiratory activity and, via sympathetic efferents, for the regulation of several elements of the cardiovascular system such as the heart, most classes of resistance arterioles, kidneys, and subsets of adrenal chromaffin cells (Guyenet, 2006).

MATERIALS AND METHODS

Animal Use

Vav3 and *Vav2* knockout mice have been described previously (Sauzeau *et al.*, 2006; Sauzeau *et al.*, 2007). H-*Ras*$^{G12V/Geo}$ knock-in animals were generated by Dr. M. Barbacid's lab (CNIO, Madrid, Spain) and reported before (Schuhmacher *et al.*, 2008). CD1, wild-type mice were used for gain-of-function experiments in culture. All animal work was carried out following the regulations set forth by both the CSIC and Salamanca University Animal Care and Use Committees. Unless otherwise indicated, we routinely used four-month-old animals for the experiments reported in this work.

Cytoarchitectural Criteria and Terminology

The terminology and abbreviations used for brain nuclei are taken from a mouse brain atlas (Frankin and Paxinos, 1996). Specifically, we considered the RVLM as the VLM region that was limited, medially, by the gigantocellular reticular nucleus and the inferior olive; laterally, by the spinal trigeminal nucleus and tract; ventrally, by the ventral medullary surface; dorsally, by the ambiguus nucleus and adjacent reticular formation; caudally, by the rostral pole of the lateral reticular nucleus; and rostrally, by the caudal pole of the facial motor nucleus. We considered as CVLM the region immediately caudal to the RVLM and that localized between the rostral wings of the lateral reticular nucleus.

Microinjection Studies

Four-month-old mice with similar body weight (20–25 g) were anesthetized with urethane (2 mg/kg body weight, Sigma, St. Louis, MO), cannulated in the carotid artery to record the evolution of arterial pressure in real time, and gently placed in a stereotaxic apparatus (Kopf, Tujunga, CA). After exposing the skull, the position of the head in the stereotaxic equipment was adjusted under the visual guidance of an operating microscope so that the height of the skull surface at the bregma and lambda was the same (Frankin and Paxinos, 1996). The interaural and midlines were taken as landmarks for the stereotaxic coordinates: for the injection in the RVLM, those were 3.05 mm caudal and 0.20 mm ventral to the interaural line and 1.20 mm lateral to the midline. For injections in the CVLM, the coordinates were 3.45 mm caudal and 0.1 mm ventral relative to the interaural line and 1.15 mm lateral to the midline. After selecting the injection area, a window in the occipital bone was drilled, and bilateral microinjections of buffered vehicle (30 nl), bicuculline (50 pmol in 30 nl, Sigma) and/or L-glutamate (100 pmol in 30 nl, Sigma) were made in the indicated VLM areas using a glass micropipette (internal diameter 40 μm) glued to a Hamilton syringe. In the case of muscimol (10 pmol in 30 nl, Sigma), the microinjections were done unilaterally. Experimental conditions (light, temperature, noises) were always kept constant during the experiments. However, to get the best comparisons, we always performed consecutive experiments of a control and a $Vav3^{-/-}$ mice in all these studies. The appropriateness of the coordinates chosen for the stereotaxic analysis was demonstrated by confirming that, as expected, the microinjection of L-glutamate in the RVLM and CVLM induce antagonistic effects in both the blood pressure and breathing rate levels. In addition, and to make it sure that the microinjection was done in the proper brainstem area in each experiment, we carried out several controls to reconfirm the targeting of the right regions within the VLM after recording the initial experimental data. First, we introduced the drugs in neighboring areas to the initial injection to confirm that the physiological response obtained in the cardiovascular and respiratory systems was restricted to the targeted VLM area (in the case of WT animals) or, alternatively, to verify that the absence of physiological responses in $Vav3^{-/-}$ mice were not due to microinjections made outside the selected VLM site (see an example in Fig. S5). Second, we microinjected in the targeted regions 30 nl of a 1% solution of Fast green FCF104022 (Merck, Darmstadt, Germany) and,

after sacrificing the mice, we obtained tissue sections from the brainstem to verify by direct microscope examination the localization of the marker (see examples in Figures 5, G and H and 7, E and F).

Tract-Tracing Experiments

Mice were anesthetized with a mixture of diazepam (5 mg/kg, Sigma), ketamine (50 mg/kg, Sigma), and atropine (1 mg/kg, Sigma). When necessary, additional anesthesia (one-fifth of the initial dose) was administered during surgery. Anesthetized animals were placed in a stereotaxic frame, their skulls exposed by a midline scalp incision, and craniotomyzed over the CVLM injection coordinates (see above). Animals received a single injection of biotinylated 10,000 Da dextran amine (Molecular Probes/Invitrogen, Carlsbad, CA) into the CVLM. To this end, a 10% dextran amine solution in saline buffer was injected iontophoretically with a 10-μm internal diameter glass micropipette using 5-μA positive current pulses (7 s on/7 s off) for 15 min. After this step, mouse scalps were sutured and animals allowed to recover for 10 d. Animals were then perfused with 4% paraformaldehyde, their brains removed, cryoprotected, and 40-μm-thick sections obtained with a freezing stage sliding microtome (Microm). Free-floating tissue sections were incubated with an avidin-biotin-peroxidase complex (ABC Standard-kit, Vector Laboratories) and the tracer revealed using as chromogen a solution containing 3,3' diaminobenzidine tetrahydrochloride and nickel ammonium sulfate. Sections were finally mounted on slides and subjected to microscopy analysis. To obtain cytoarchitectonic references, a series of sections were counterstained in parallel with 0.1% cresyl violet (Merck). The dextran amine-labeled fibers, collaterals, and varicosities were studied using a PL Fluotar $\times$40 lens (Leica, Wetzlar, Germany) attached to a DMRB light microscope (Leica) that, in turn, was connected to a computer running the Neolucida software (MicroBrightField, Williston, VT). A set of seven sections of the VLM from the same animal, regularly spaced at 160 μm, were drawn and reconstructed in three dimensions to compare the distribution of dextran amine-labeled fibers in $Vav3^{-/-}$ and control animals. The external contour of medulla, boundaries of the central canal, as well as the nucleus ambiguus and the needle wound area were recorded for spatial reference purposes. Chartings of each section made were plotted, scaled down, and arranged into plates with the Corel-DRAW X3 software (Corel, Ottawa, Canada). Three-dimensional reconstructions were displayed and analyzed using the Neuroexplorer program (MicroBrightField).

Isolation and Transfection of Hippocampal GABAergic Cells

Hippocampi from CD1, $Vav3^{+/+}$, and $Vav3^{-/-}$ mice were obtained (Bamji *et al.*, 2003; Rico *et al.*, 2004), cells cultured in poly-L-lysine (0.5 mg/ml) and, when appropriate, transfected as described previously (Chacon *et al.*, 2010). For gain-of-function experiments, pcDH1-MCS1-EF1-CoGFP vectors (System Biosciences) encoding either wild-type Vav3 (pCQS1) or a constitutively active Vav3 protein (Δ1–144 deletion, pCQS3) were transfected at 2 DIV into ICR hippocampal neurons. As control, we used the empty pcDH1-MCS1-EF1-CoGFP vector. For loss-of-function experiments, a mammalian plasmid (pCS2-EGFP; Clontech) encoding the enhanced green fluorescent protein (EGFP) was transfected into both wild-type and $Vav3^{-/-}$ hippocampal cultures. We chose this timing of transfection to specifically interfere with the elaboration of axons, but not with their initial outgrowth (Chacon *et al.*, 2010). Cells were examined at 5 DIV. When appropriate, cells were stimulated with EphrinA1 (5 μg/ml, R&D, Minneapolis, MN) for 10 min, fixed, and processed as above.

Immunocytochemistry of Hippocampal Cultures

For immunocytochemistry, neuronal cultures were fixed with 4% paraformaldehyde for 20 min at room temperature, treated with 0.25% Triton X-100 for 10 min, and blocked in a solution containing 2% normal goat serum (Atom, Barcelona, Spain) and 2% bovine serum albumin in phosphate-buffered saline solution for 30 min. After overnight incubation at 4°C with primary antibodies, cells were rinsed with phosphate-buffered saline solution and incubated with Alexa488-, Alexa594-/Alexa555-, or Alexa633 secondary antibodies to either mouse or rabbit IgGs (Molecular Probes/Invitrogen) for 1 h. Primary antibodies included a mouse mAb to GAD65 (Sigma), a rabbit polyclonal to GABA (Sigma), and the home-made rabbit polyclonal antibody to Vav3 (Movilla and Bustelo, 1999).

All pictures were acquired using a DC500 Leica camera attached to a Leica CTR5000 microscope (Leica Microsystems; $\times$20/0.5 HC PL Fluotar). All images were captured under the same conditions within each type of experiment. When quantitation was required, selected images were exported to Image J (National Institutes of Health, NIH software). The longest neurite per neuron was measured. GABA-positive growth cone areas were calculated by tracing those structures on the corresponding microscope image. Then, the percentage of collapsed growth cones was analyzed in pictures taken within a cross-shape field traced in each experimental coverslip.

Statistical Analysis

Data from $Vav3^{-/-}$ and control animals were analyzed using ANOVA (Figures 1, 4, 7, and left histogram of 8D), 1-tailed Student's t (Figure 3 and Supplemental Figures S1–S4), nonparametric Mann–Whiney (right histogram

of Figure 8, D, F, and left histogram in H), and χ^2 (Figure 8H, right panel) tests. Data are given as the mean ± the SEM. *P* values lower than 0.05 were considered as statistically significant.

Other experimental procedures can be found in the Supplemental Information.

RESULTS

The Vav3-Deficiency Does Not Affect the Mechanoelastic and Signaling Properties of Blood Vessels

To investigate the cause of the SNS/AngII-dependent hypertension of Vav3-deficient mice, we first focused our attention on the mechanoelastic behavior of blood vessels and the signaling properties of vascular smooth muscle cells. Using a number of physiological and signaling experiments, we found that the high blood pressure and SNS hyperactivity of *Vav3*⁻/⁻ mice were not caused by intrinsic mechanical or signal reactivity problems in arterial vessels (see Supplemental Text and Supplemental Figures S1–S3). Furthermore, we have previously shown that inactivation of the *Vav3* gene, unlike the case of the *Vav2* locus, does not eliminate the response of vascular smooth muscle cells to nitric oxide and, therefore, that these mice have normal vasodilation to nitric-oxide-dependent stimuli (Sauzeau *et al.*, 2010). Histo-

logical analysis of the adrenal medulla also ruled out the presence of pheochromocytoma (data not shown), an adrenal gland-derived tumor that raises catecholamine levels and blood pressure in humans (Lenders *et al.*, 2005). These results, together with the previous observation that the renal defects of *Vav3*⁻/⁻ mice were a consequence of the hypertensive condition found in these animals (Sauzeau *et al.*, 2006), indicated that the origin of the hypertension and SNS hyperactivity of these animals was not due to peripheral defects in the renovascular system.

Vav3 Loss Leads to Tachypnea

A more comprehensive characterization of the phenotype of *Vav3*⁻/⁻ mice revealed that these animals suffered from tachypnea under normoxia (Figure 1, A and B). They also displayed dysfunctional respiratory responses to environmental challenges. Thus, whereas wild-type (WT) animals responded to hypercapnia with an initial increase in both the frequency and amplitude of the inspiration/expiration cycles that was followed by a rapid deceleration of breathing activity (Figure 1C), *Vav3*⁻/⁻ animals did not change significantly their accelerated breathing frequencies through-
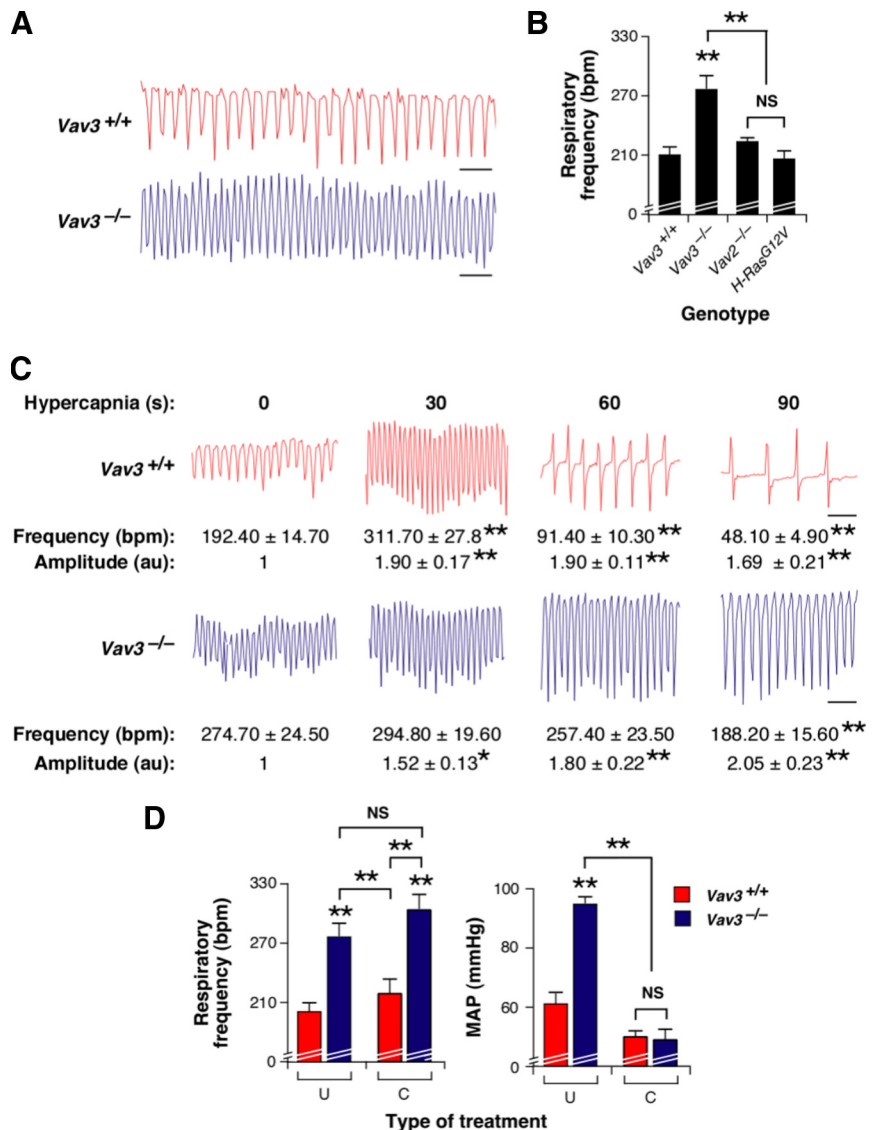

Figure 1. *Vav3*⁻/⁻ mice show abnormal breathing patterns. (A) Example of representative real-time recordings of the respiratory frequency of a WT and a *Vav3*⁻/⁻ mouse. Upward and downward deflections represent inspiration and expiration movements, respectively. Scale bar, 1 s. (B) Quantitation of respiratory frequency rates in mice of indicated genotypes (n = 10–17). bpm, breaths per min; **p < 0.01 compared with control animals or the indicated experimental pair (in brackets). NS, not statistically significant. (C) Representative segments of the breathing response of a WT and a *Vav3*⁻/⁻ mouse subjected to hypercapnia for the indicated periods of time. Scale bar, 1 s. Values below each chart indicate the mean and SEM of the respiratory frequency and amplitude at the indicated times of the hypercapnia response (n = 6). au, arbitrary units. *p < 0.05; **p < 0.01 compared with WT controls. (D) Comparison of the respiratory frequency (left panel, n = 6–9) and mean arterial pressure (MAP) (right panel, n = 6–9) of animals of the indicated genotypes that were either left untreated (U) or treated with captopril (C) as indicated in Supplemental Materials and Methods. **p < 0.01 compared with either untreated WT controls or the indicated experimental pair (in brackets).

out the hypercapnic conditions (Figure 1C). Several observations demonstrated that the tachypnea, unlike other dysfunctions found in these animals (Sauzeau *et al.*, 2006), was not due to the hypertensive state present in these animals. Thus, we observed that $Vav2^{-/-}$ knockout and H-$Ras^{G12V/G12V}$ knock-in animals, two mouse strains that develop an AngII-dependent hypertensive state (Sauzeau *et al.*, 2007; Schuhmacher *et al.*, 2008), had normal breathing rates under both normoxic (Figure 1B) and hypercapnic conditions (data not shown). Furthermore, we found that a long-term treatment with captopril, a drug that blocks AngII biosynthesis and the hypertensive state of $Vav3^{-/-}$ mice (Figure 1D) (Sauzeau *et al.*, 2006), did not have any effect in the tachypnea present in Vav3-deficient animals (Figure 1D). Additional experiments ruled out that the hypercapnia could induce the hypertension of $Vav3^{-/-}$ animals due to defective O_2/CO_2 exchange in their lungs (see Supplemental Text, Supplemental Table S1, and Supplemental Figure S4). These results indicate that the Vav3 mutation leads to general, mutually independent dysfunctions in the control of blood pressure and respiratory rates.

Vav3 Is Expressed in GABAergic Cells of the Ventrolateral Medulla

The simultaneous development of chronic sympathoexcitation, tachycardia, systemic hypertension, and tachypnea in Vav3-deficient mice suggested that they probably had a neurogenic defect in regulatory centers controlling sympathetic outflow as well as cardiovascular and respiratory activities. To shed light on the possible origin of the phenotype of $Vav3^{-/-}$ mice, we next performed expression studies to localize the sites of expression of the *Vav3* proto-oncogene in mouse tissues. These analyses indicated that *Vav3* was present in cerebellar granular and Purkinje cells (Quevedo *et al.*, 2010), scattered neurons of the prefrontal cortex, and GABAergic cell populations of the hippocampus (see below, Figure 8, A and B). Interestingly, Vav3 was detected at high levels in both the rostral (RVLM) and caudal (CVLM) parts of the VLM (Figure 2), a brainstem center involved in the regulation of heart, vascular, and respiratory activity (Bianchi *et al.*, 1995; Richter and Spyer, 2001; Guyenet, 2006). To ensure properly balanced physiological responses, the sympathetic outflow of RVLM neurons is regulated by GABAergic (inhibitory) and glutamatergic (excitatory) inputs (Guyenet, 2006). The inhibitory inputs on the RVLM emanate primarily from GABAergic neurons present in the CVLM whereas the glutamatergic signals derive form other brain areas (Blessing, 1988; Thrasher, 2005; Guyenet, 2006). Within the VLM, we detected high levels of Vav3 protein (Figure 2, A–D) and *Vav3* mRNA (Figure 2C) in somas of CVLM cells. We could not detect the *Vav3* transcript in the RVLM (Figure 2C). However, we did observe that its encoded
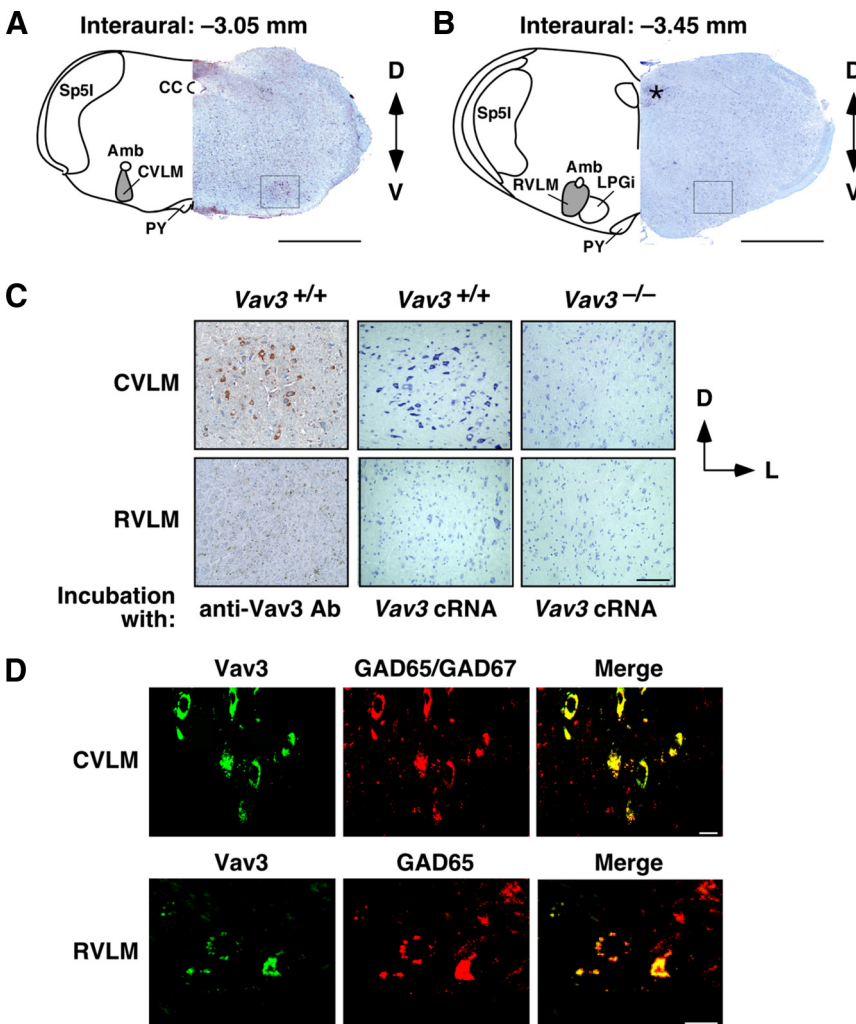

Figure 2. Expression of Vav3 in the VLM. (A and B) Representative examples of coronal brainstem sections containing either the CVLM (A) or the RVLM (B) that were processed to detect the expression of the Vav3 proto-oncogene. On the left side of each panel, selected anatomical areas have been highlighted. Amb, nucleus ambiguus; CC, central canal; LPGi, lateral paragigantocellular nucleus; PY, pyramidal tract; Sp5I, spinal trigeminal nucleus interpolar. VLMs are shaded on gray. In the right side of each panel, we show a hematoxylin-eosin stained section incubated with anti-Vav3 antibodies. *nonspecific signal; D, dorsal; V, ventral. Squares show areas considered to contain the CVLM (A) and RVLM (B). Scale bar, 1 mm. (C) Detection of either Vav3 protein (left panels) or *Vav3* mRNA (rest of panels) in VLM areas from mice of the indicated genotypes. Scale bar, 100 μm. Ab, antibody; cRNA, antisense cRNA probe; L, lateral. (D) Colocalization of Vav3 (green, left panels) with GAD65 and GAD67 (red, middle panels) in the indicated VLM areas by confocal immunofluorescence. Areas of colocalization are shown in yellow (right panels). Scale bar, 10 μm.

product displayed a characteristic punctate pattern in that region (Figure 2, C and D). These signals were not seen in sections from $Vav3^{-/-}$ mice (Figure 2C), demonstrating they were specific for Vav3. Vav3 colocalized with the GABAergic markers GAD65 and GAD67 in the cytosol of cells present in the CVLM (Figure 2D). In the RVLM, Vav3 also colocalized with GAD65, a marker for presynaptic GABAergic terminals, in vesicle-like structures (Figure 2D). These results indicate that the expression of Vav3 is restricted to the somas and axon terminals of CVLM GABAergic neurons, the cell type of the CVLM that relays both tonic and baroreceptor-dependent inhibitory signals to RVLM cells (Guyenet, 2006).

Defective GABAergic Responses in the Ventrolateral Medulla of $Vav3^{-/-}$ Mice

In light of the above expression profile, we decided to study the functional status of the VLM in $Vav3^{-/-}$ mice. Using immunofluorescence techniques, we observed a marked reduction ($\approx$50%) in the expression of specific GABAergic axon terminal markers, including GAD65 (Figure 3, A and B) and v-GAT (Figure 3, A and B) in the RVLM of $Vav3^{-/-}$ mice when compared with WT animals. In contrast, we did not detect any change in the expression of GABA$_A$ receptors in this area (Figure 3, A and B). In agreement with the loss of inhibitory synapses, immunohistochemical analyses revealed that the RVLM of $Vav3^{-/-}$ animals contained neurons with higher levels of tyrosine hydroxylase immunostaining density than those from control mice (Figure 3, B–D), a clear indication of catecholaminergic hyperactivity in the RVLM of Vav3-deficient animals. These results suggested that the up-regulation of the SNS found in $Vav3^{-/-}$ mice might derive from the reduction in the number of GABAergic inputs that exert inhibitory modulation on postsynaptic RVLM cells.

To validate this hypothesis, we tested in vivo the GABAergic and glutamatergic responses of the VLM using stereotaxic methods. The stereotaxic coordinates selected for the RVLM and CVLM in these experiments (see Materials and Methods) were accurate, as demonstrated by the expected responses induced by microinjections of L-glutamate in the RVLM (increase in blood pressure and breathing frequency; see Supplemental Figure S5, A–C), CVLM (reduction in blood pressure and bradypnea, see Supplemental
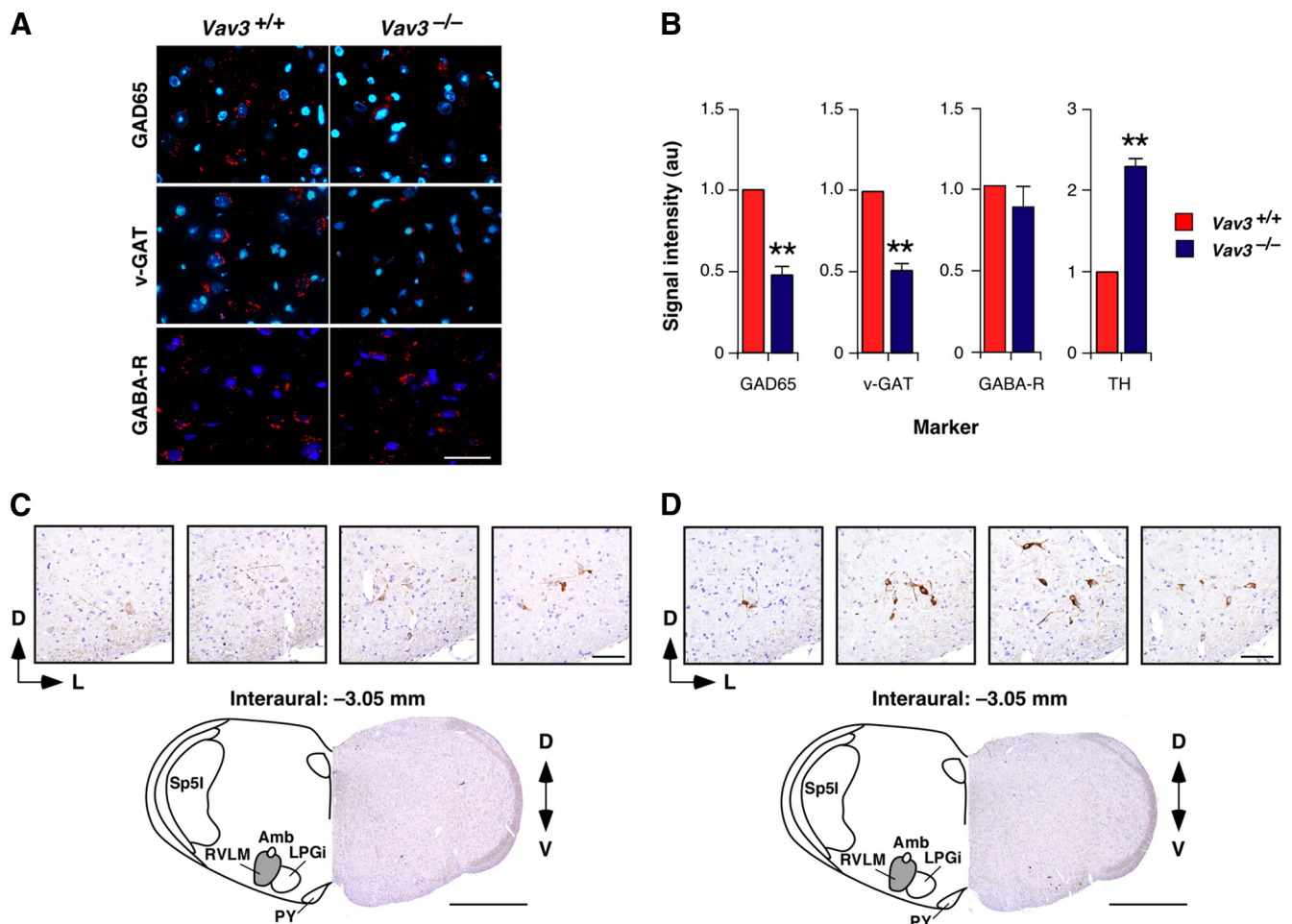

Figure 3. Vav3 affects the number of GABAergic inputs in the RVLM. (A) Detection of GAD65 (top panels), v-GAT (middle panels), and GABA$_A$ receptor (GABA-R, bottom panels) in WT (left panels) and $Vav3^{-/-}$ (right panels) RVLMs using immunofluorescence techniques. Cell nuclei were visualized using DAPI. Scale bar, 40 μm. (B) Intensity levels of the signals for each maker in the RVLM sections from mice of the indicated genotypes (n = 7–10). **p < 0.01 compared with WT controls. (C and D) Top, expression of tyrosine hydroxylase in coronal sections of the brainstem containing the RVLM from WT (C) and $Vav3^{-/-}$ (D) mice. Sections were taken serially from a more rostral (left) to a more caudal (right) position within the RVLM. Bottom, representative coronal brainstem sections from a WT (C) and a $Vav3^{-/-}$ (D) mouse. The position of these sections is the same to those shown in the third panel displayed at the top. Abbreviations of brainstem areas are the same used in the legend to Figure 2. Scale bars: 100 μm (top panels) and 1 mm (bottom panels).

Figure S5, D–F), and in an area outside the VLM (no effect on those two parameters, see Supplemental Figure S5, G–I) of WT mice. We then microinjected in the RVLM bicuculline, a GABA$_A$ receptor inhibitor that promotes high blood pressure and accelerated breathing by blocking the inhibitory effects of GABA on RVLM neurons (Yoshida *et al.*, 2002). We reasoned that if our hypothesis were correct, $Vav3^{-/-}$ animals would show a reduced response to bicuculline when compared with their normal littermates. The microinjection of this drug in the RVLM induced a rapid and transient increase in both the blood pressure (Figure 4, A and B) and breathing frequency (Figure 4, C and D) in WT but not $Vav3$ null animals. The plasma concentration of SNS-derived noradrenaline and adrenaline also increased in $Vav3^{+/+}$ mice (Figure 4, E and F) but either did not change (in the case of noradrenaline, Figure 4E) or increased to a much lower extent

(in the case of adrenaline, Figure 4F) in $Vav3^{-/-}$ animals under these experimental conditions, further demonstrating that the GABAergic responsiveness of the RVLM was altered in Vav3-deficient mice. By contrast, we observed that the subsequent microinjection of L-glutamate in the same brainstem region promoted surges in the blood pressure (Figure 4, A and B) and breathing frequency (Figure 4, C and D) in animals of both genotypes, indicating that the response of VLM cells to this neurotransmitter was not altered in the knockout animals. We also observed that $Vav3^{-/-}$ and control animals reacted to microinjections of L-glutamate alone in the RVLM with increases in blood pressure, breathing rates, and catecholamine plasma levels (Supplemental Figure S5, A–C and data not shown). Despite this, we routinely observed that the high blood pressure generated under these conditions lasted twice as long in Vav3-deficient mice than in WT animals (Figure 4G),
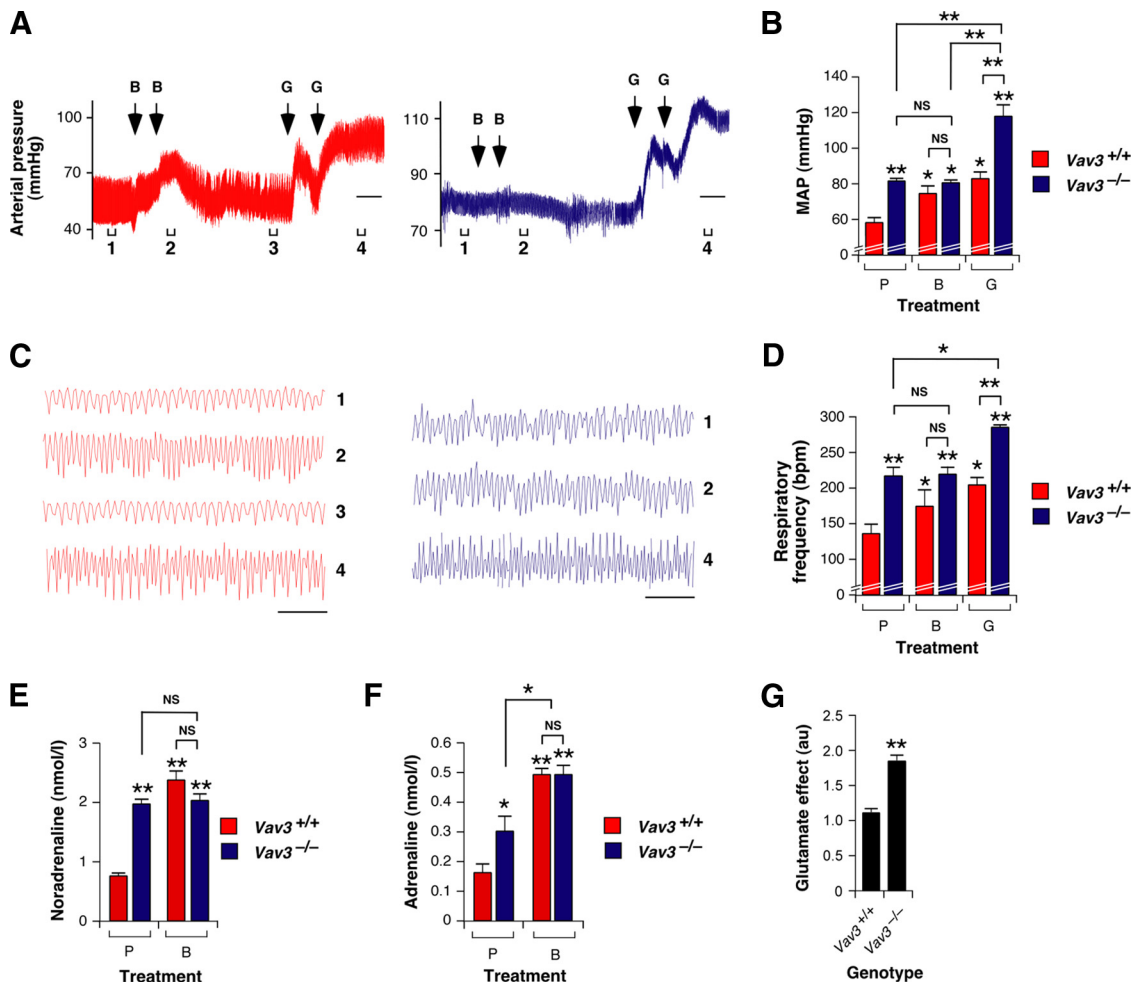

Figure 4. GABAergic signal defects in the RVLM of $Vav3^{-/-}$ mice. (A) Representative real-time recordings of the blood pressure levels of a WT (red, left panel) or a $Vav3^{-/-}$ (blue, right panel) mouse upon bilateral microinjections of bicuculline (B) and L-glutamate (G) in the RVLM. The time of injection is indicated by arrows. Brackets (labeled 1–4) shown at the bottom of charts indicate the time intervals for the breathing recordings shown in C. Intervals 2 and 4 were also used to measure the drug-induced arterial pressure shown in panel B. Scale bar, 2 min. (B) Arterial pressure levels in animals of the indicated genotypes microinjected in the RVLM with bicuculline (B) and L-glutamate (G) or with placebo (P) (n = 5–6). *p < 0.05; **p < 0.01 compared with either the untreated WT controls or the indicated experimental pair (in brackets). (C) Example of representative real-time recordings of the respiratory frequency of a WT (red, left panel) and a $Vav3^{-/-}$ (blue, right panel) mouse at the times indicated in panel A. (D) Breathing frequency in mice of the indicated genotypes subjected to the microinjections shown in B (n = 5–6). *p < 0.05; **p < 0.01 compared with either the untreated WT controls or the indicated experimental pair (in brackets). (E and F) Bicuculline-dependent variations in the plasma levels of noradrenaline (E) and adrenaline (F) in mice of the indicated genotypes (n = 5). *p < 0.05; **p < 0.01 compared with either untreated WT animals or the indicated experimental pair (in brackets). (G) Time of recovery of the blood pressure upon the bilateral microinjection of L-glutamate in the RVLM of mice of the indicated genotypes (n = 5–6). **p < 0.01 compared with WT control.

suggesting that the L-glutamate excitatory effect in the RVLM was not counterbalanced adequately by GABAergic signals in the case of $Vav3^{-/-}$ mice.

The functionality of postsynaptic GABA receptors was not affected in the RVLM of Vav3-deficient mice, because we observed a similar drop in blood pressure (Figure 5, A and B) and breathing frequency (Figure 5, C and D) in $Vav3^{-/-}$ and WT animals upon the microinjection of muscimol, a GABA receptor agonist, in the RVLM. These results are consistent with the prior observation that RVLM neurons have normal levels of $GABA_A$ receptors in $Vav3^{-/-}$ animals (see above, Figure 3, A and B). Supporting the hypothesis
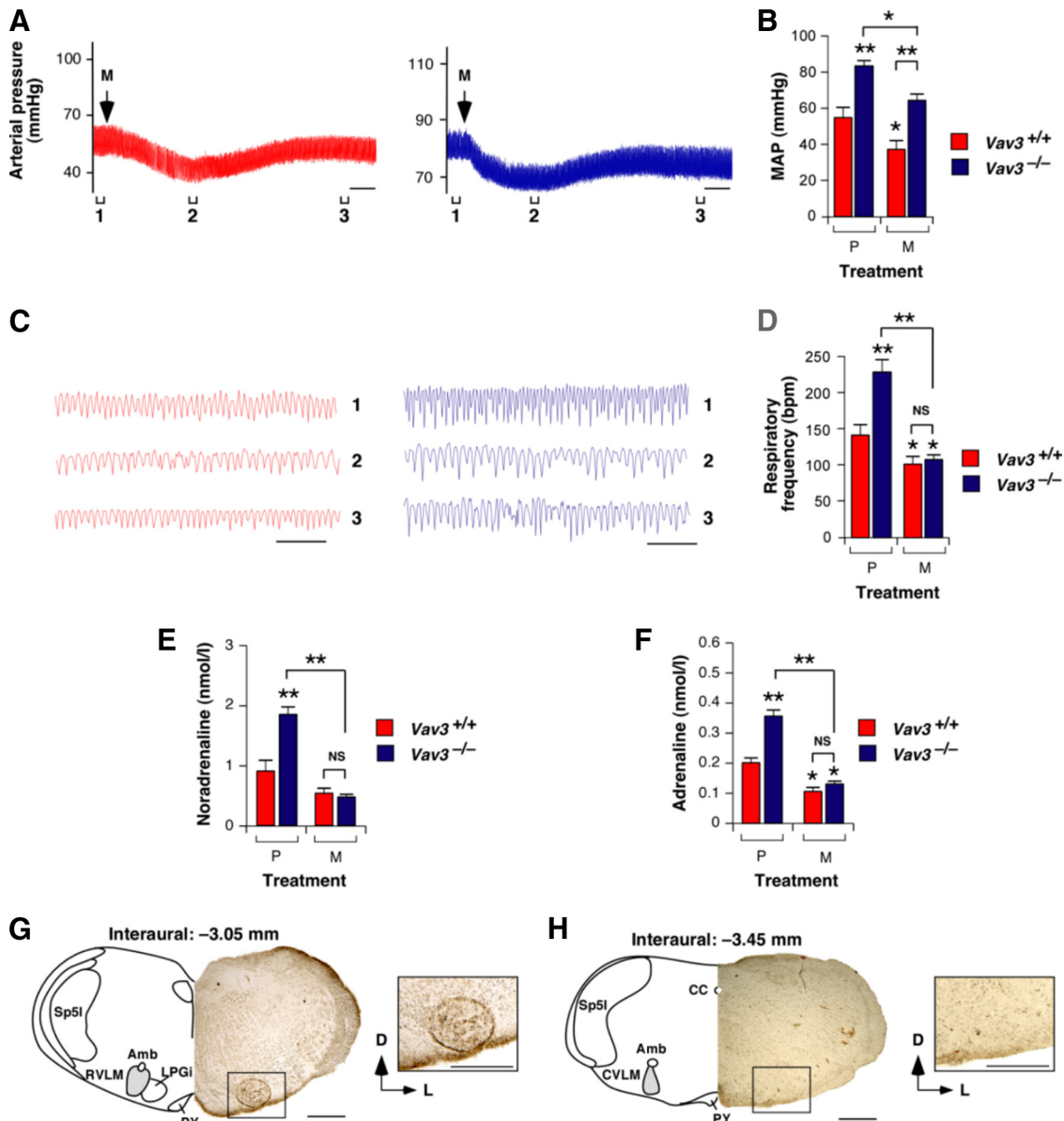

Figure 5. Normal response of the RVLM of $Vav3^{-/-}$ mice to muscimol. (A) Representative real-time recordings of blood pressure levels in a WT (red, left panel) or a $Vav3^{-/-}$ (blue, right panel) mouse upon unilateral microinjections of muscimol (M) in the RVLM. The time of injection is indicated by arrows. Brackets (labeled 1–3) shown at the bottom of charts indicate the time intervals for the breathing recordings shown in C. Segments 2 were also used to measure the drug-induced arterial pressure shown in panel B. Scale bar, 2 min. (B) Arterial pressure levels in animals of the indicated genotypes microinjected in the RVLM with muscimol (M) or placebo (P) (n = 5–6). *p < 0.05; **p < 0.01 compared with either untreated WT mice or the indicated experimental pair (in brackets). (C) Example of representative real-time recordings of the respiratory frequency of a WT (red, left panel) and a $Vav3^{-/-}$ (blue, right panel) mouse at the times indicated in panel A. (D) Breathing frequency of mice of the indicated genotypes subjected to the microinjections indicated in B (n = 5–6). *p < 0.05; **p < 0.01 compared with either untreated WT control or the indicated experimental pair (in brackets). (E and F) Muscimol-dependent variations in the plasma levels of noradrenaline (E) and adrenaline (F) in mice of the indicated genotypes (n = 5). *p < 0.05; **p < 0.01 compared with either untreated WT mice or the indicated experimental pair (in brackets). (G and H) Example of the appropriate localization of the microinjected Fast green FCF104022 marker in the RVLM of a $Vav3^{-/-}$ mice. A Fast green solution (30 nl) was microinjected in the RVLM of mice. After euthanasia, coronal brainstem sections containing either the RVLM (G) or the CVLM (H) were generated and processed to detect Fast green signals. A schematic representation of the brainstem in those sections has been included in the panels for reference purposes. Abbreviations of brainstem areas are the same used in the legend to Figure 2. Scale bars, 0.5 mm.

that the sympathoexcitation is a downstream effect of the deregulated activity of the RVLM, we observed that the microinjection of muscimol in this region eliminated the high levels of catecholamines present in the plasma of Vav3-deficient mice (Figure 5, E and F). In addition to the expected physiological responses obtained with the microinjection of L-glutamate and muscimol in the RVLM of $Vav3^{-/-}$ mice (see above), the injection of the Fast green FCF104022 marker confirmed that the microinjections did target the RVLM and not other cardiorespiratory centers in the brainstem such as the CVLM (Figure 5, G and H). Taken together, these results indicate that the RVLM of $Vav3^{-/-}$ mice does not respond correctly to GABAergic inhibitory inputs that modulate catecholamine production, blood pressure, and respiratory activity.

Abnormal GABAergic Connectivity between the CVLM and RVLM

The reduction of GABAergic inputs and the dysfunction of GABAergic-mediated responses in the RVLM of $Vav3^{-/-}$ animals could be due to a reduction in the number of GABAergic CVLM neurons, to axon guidance defects, and/or to improper synapse formation by the GABAergic axons once they reached the bulbospinal VLM postsynaptic targets. To identify the cause of the GABAergic dysfunction present in $Vav3^{-/-}$ mice, we first evaluated by immunohistochemistry the relative numbers of GABA-positive cells in the VLM of both Vav3-deficient and control animals. These experiments revealed similar densities of GABA-positive cells in the VLMs regardless of the genotype of the animals

examined (Supplemental Figure S6), indicating that the development, survival, and/or migration of GABAergic cells to the CVLM was not grossly affected by the loss of *Vav3* gene expression.

To investigate the status of the GABAergic axon projections from the CVLM to the RVLM, we next introduced biotinylated dextran amine, a predominantly anterograde neurotracer (Reiner *et al.*, 2000), in CVLM-localized cells using iontophoretic techniques. After a period of recovery to allow the migration of the tracer along the axons of the iontophoresed cells, we killed the animals and studied the localization of dextran amine-labeled axon fibers and terminals in serial brainstem sections. Costaining of some of those sections with GABAergic markers (GAD65 and GAD67) demonstrated that the neurotracer was effectively introduced in a significant fraction of CVLM GABAergic cells (Supplemental Figure S7). As expected, the tracer was also introduced in non-GABAergic cells (Supplemental Figure S7). In WT animals, we observed that the tracer migrated from the injection site to the RVLM following both ipsilateral and contralateral routes (Figure 6, A and B). This bilateral migration pattern is consistent with previously analysis conducted in the VLM using axon tract-tracing and physiological methods (Li *et al.*, 1991; Masuda *et al.*, 1991; Schreihofer and Guyenet, 2003). Other rostral and caudal projections from the injection site were also observed (Figure 6, A and B and Supplemental Text), a result that confirms previous data indicating that CVLM neurons establish connections with several regions of the brainstem (see Supplemental Text). We observed the same migration routes for the
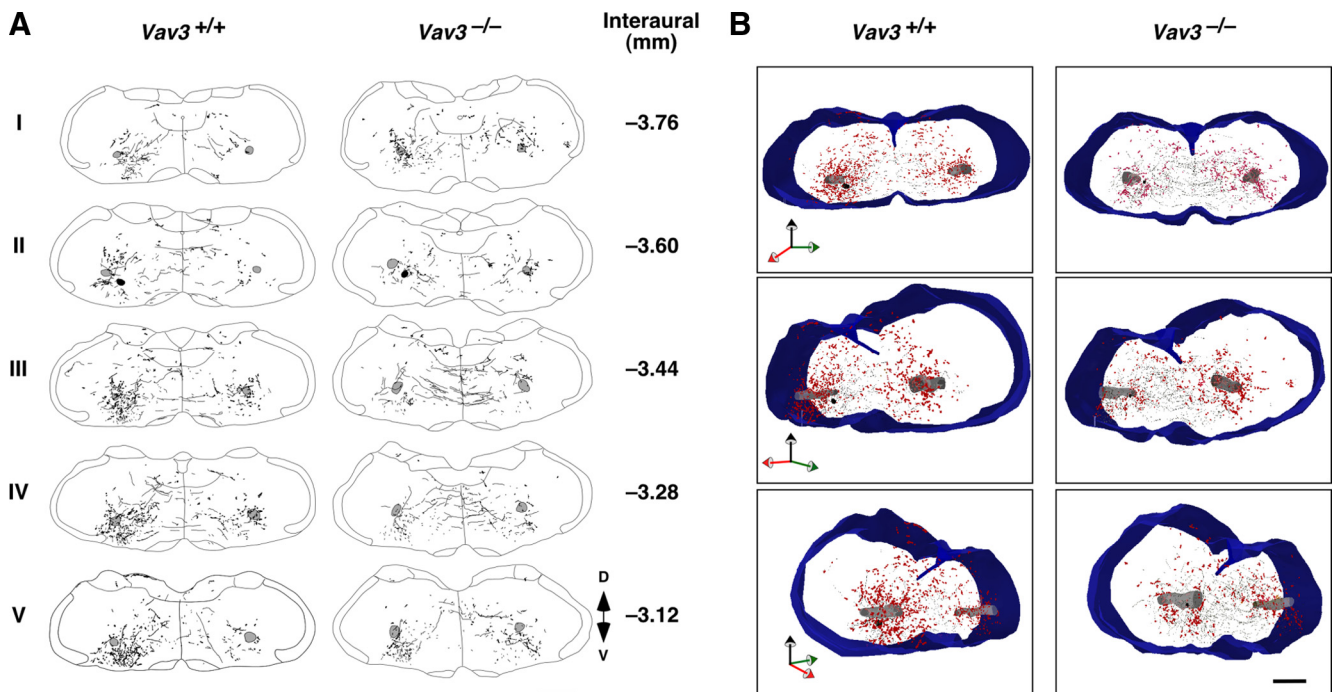

Figure 6. Defects in axon guidance in the VLM of $Vav3^{-/-}$ mice. (A) Distribution of dextran amine-labeled fibers (lanes) and buttons (dots) in coronal brainstem sections derived from mice of the indicated genotypes. Sections shown were taken in the original dextran amine injection site (II) as well as in either more caudal (I) or rostral (III–V) positions from that injection site (n = 4 in each group). Scale bar, 500 μm. The area shaded on black in section II marks the neurotracer injection site. The area shaded on gray indicated the position of the nucleus ambiguus used for orientation purposes. The coordinates of each section are indicated on the right. (B) 3D reconstruction of the trajectory and localization of dextran amine-labeled fibers (black) and buttons (red dots). A frontal (upper panels), a 45° rotation to the left (middle panels), and a 45° rotation to the right (bottom panels) view is displayed for each data group collected from WT (left column) and $Vav3^{-/-}$ (right column) mice. The injection site (black sphere), the nucleus ambiguus (gray cylinders), and the external contour and central canal (blue) have been highlighted in all 3D reconstructions. Scale bar, 500 μm.

neurotracer in the case of brainstem sections obtained from $Vav3^{-/-}$ mice. However, we reproducibly detected in this case a reduced number of dextran amine-positive buttons in sections located before and on the RVLM itself (Figure 6, A and B). Several observations indicated that this was not due to less effective iontophoretic efficiencies of the experiments involving knockout animals. First, we consistently observed the same reduction in four independent tract-tracing experiments. Second, we observed that the reduction in buttons and fibers did not affect other regions of the $Vav3^{-/-}$ brainstem. For example, we reproducibly observed a significant increase in the number of dextran amine-positive buttons in sections located caudally to the injection site in Vav3-deficient mice when compared with samples from control animals (Figure 6, A and B; top panels on the right). Likewise, we observed an increase in the number of dextran-amine–labeled fibers crossing between the ipsilateral and contralat-

eral injection side in sections immediately rostral to the injection site in $Vav3^{-/-}$ animals relative to WT mice (Figure 6A, third and fourth panels from top). We also confirmed by histological analysis that the scar of the needle used for the iontophoresis was accurately located in the CVLM (Figure 6A, second panels from top). These observations indicate that the loss of Vav3 induces improper innervation of the RVLM postsynaptic targets by CVLM GABAergic cells.

To corroborate the above data with independent techniques, we decided to record the transmission of GABAergic signals from the CVLM to the RVLM. To this end, we took advantage of previous observations indicating that the addition of L-glutamate stimulates the GABAergic cells present in the CVLM (Tolentino-Silva *et al.*, 2000). Consistent with this, we observed that microinjections of L-glutamate in the CVLM induced a rapid, but transient reduction in the blood pressure (Figures 7, A and B, and Supplemental Fig-
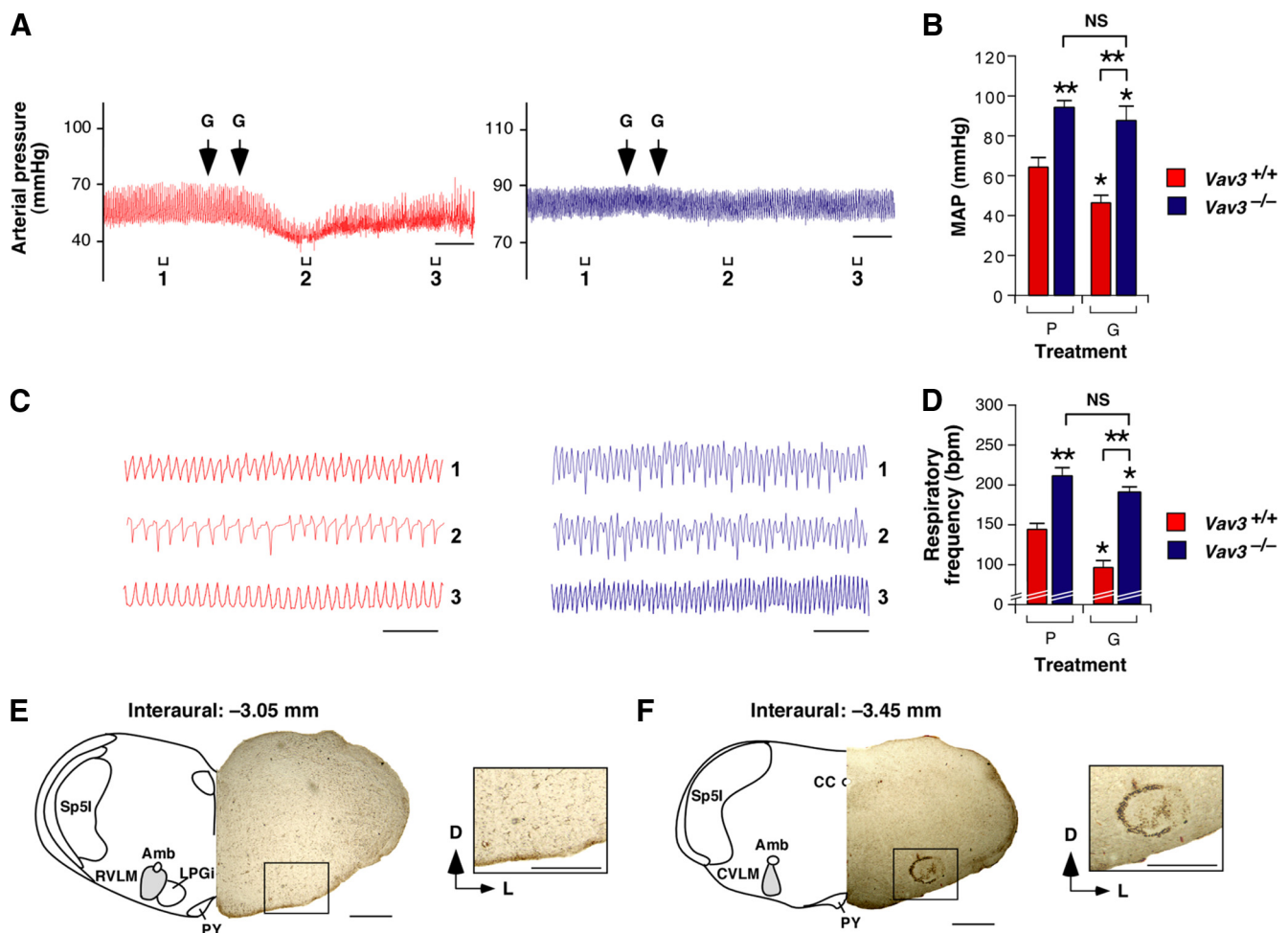

Figure 7. Defects in GABAergic transmission in the VLM of $Vav3^{-/-}$ mice. (A) Representative real-time recordings of blood pressure levels of a WT (red, left panel) or a $Vav3^{-/-}$ (blue, right panel) mouse upon a bilateral microinjection of L-glutamate (G) in the CVLM. The time of each microinjection is indicated by arrows. Brackets (labeled 1–3) shown at the bottom of charts indicate the time intervals for the breathing recordings shown in C. Segments 2 were also used to measure the drug-induced arterial pressure shown in panel B. Scale bar, 2 min. (B) Arterial pressure levels in animals of the indicated genotypes microinjected in the CVLM with L-glutamate (G) or placebo (P) (n = 5–6). *p < 0.05; **p < 0.01 compared with either untreated WT mice or the indicated experimental pair (in brackets). (C) Example of representative real-time recordings of the respiratory frequency of a WT (red, left panel) and a $Vav3^{-/-}$ (blue, right panel) mouse at the times indicated in panel A. Scale bar, 2 s. (D) Breathing frequency in mice of the indicated genotypes microinjected in the CVLM with either L-glutamate (G) or placebo (P) (n = 5–6). *p < 0.05; **p < 0.01 compared with either untreated WT mice or the indicated experimental pair (in brackets). (E,F) Example of the appropriate localization of the microinjected Fast green FCF104022 marker in the CVLM of a $Vav3^{-/-}$ mice. On microinjection of the marker, coronal brainstem sections containing the RVLM (E) and the CVLM (F) were obtained and processed as indicated in Materials and Methods. Abbreviations of brainstem areas are the same used in the legend to Figure 2. Scale bars, 0.5 mm.
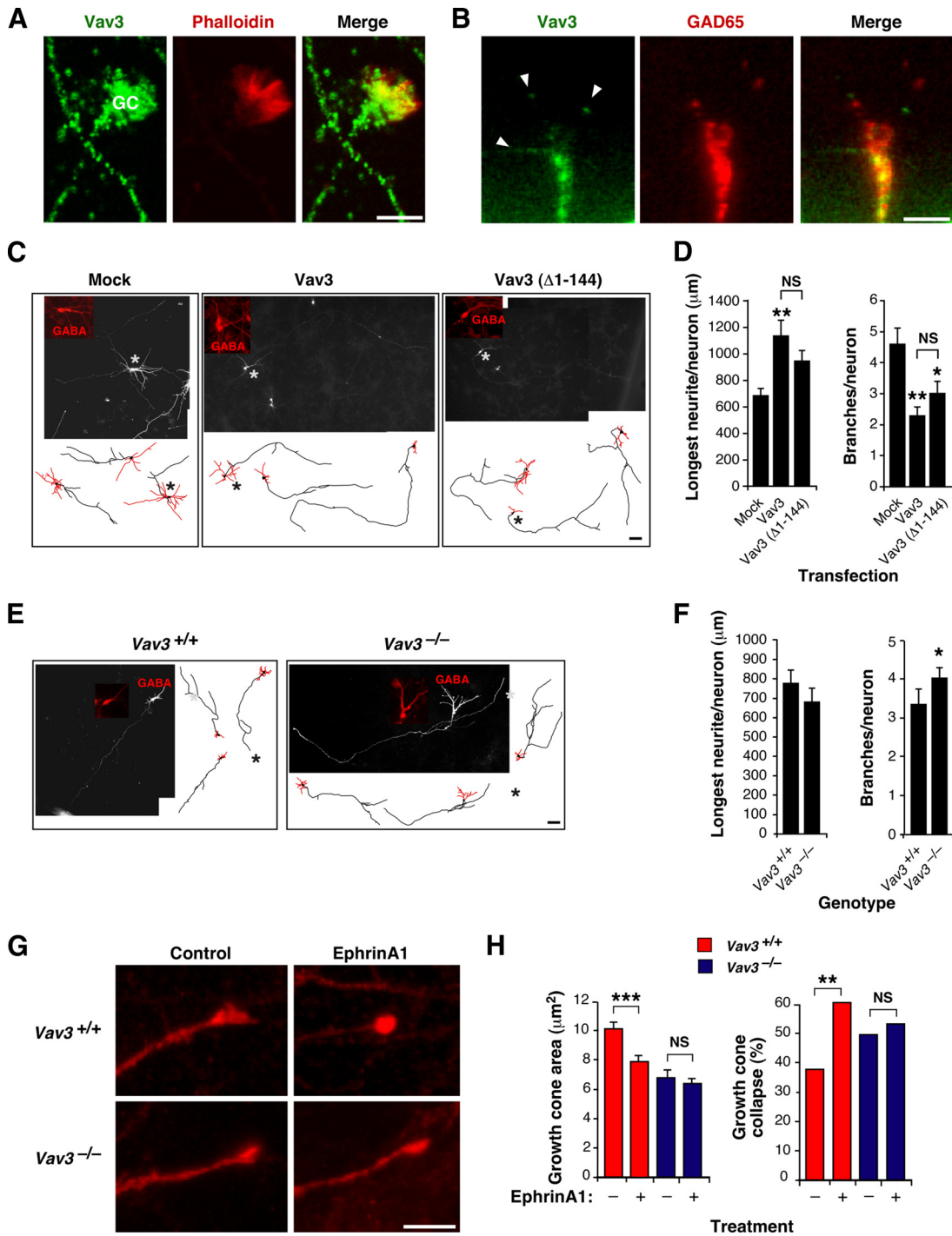
Figure 8. Vav3 controls axon growth and branching in GABAergic cells. (A and B) Detection of the indicated proteins (top) in WT hippocampal GABAergic neurons in culture by either standard (A) or confocal (B) microscopy. Signals derived from Vav3 are shown in green (A and B; left and right panels). Phalloidin (A) and GAD65 (B) staining are shown in red (middle and right panels). Areas of colocalization of Vav3 with the other two proteins are shown in yellow (A and B; right panels). GC, growth cone (A). Arrowheads indicate the localization of Vav3 in tips of filopodia (B). Scale bar, 5 μm. (C) Composite images and representative drawings of 5 DIV WT GABAergic hippocampal neurons (red) that were mock-transfected (left panel) or transfected with plasmids encoding the indicated Vav3 proteins (top). Scale bars, 40 μm (images) and 80 μm (drawings). (D) Quantification of the longest neurite length per neuron (n = 99 neurons, three independent experiments) (left panel) and of number of branches per neuron (n = 99 neurons, three independent experiments) (right panel). *p < 0.05; **p < 0.01 compared with either mock-transfected cells or the indicated experimental pair (in brackets). (E) Composite images and representative drawings of WT (left panel) and Vav3-deficient (right panel) hippocampal GABAergic neurons (identified in red using anti-GABA antibodies). Scale bar as in B. (F) Quantification of the longest neurite length per neuron (n = 104 neurons, three independent experiments) (left panel) and of branches per neuron (n = 104 neurons, three independent experiments) (right panel). *p < 0.05 compared with WT cells. (G) Images of WT (upper panels) and Vav3-deficient (lower panels) hippocampal GABAergic growth cones upon incubation of 5 DIV cell cultures with either control (left panels) or EphrinA1-containing (right panels) media for 10 min. Scale bar, 5 μm. (H) Quantification of the growth cone area (n = 546 growth cones, three independent experiments) (left panel) and collapse (n = 546 growth cones, three independent experiments) (right panel) in the total population of neurons identified as GABA positive neurons in the indicated culture conditions. **p < 0.01; ***p < 0.01 compared with the indicated experimental pair (in brackets).

ure S5E) and respiratory activity (Figures 7, C and D and Supplemental Figure S5F) of WT animals. By contrast, the microinjection of this neurotransmitter had no significant effects in the blood pressure (Figure 7, A and B) and breathing rates (Figure 7, C and D) of $Vav3^{-/-}$ mice, further supporting the lack of proper GABAergic innervation of the RVLM by the CVLM in those mice. Subsequent controls microinjecting the Fast green FCF104022 marker in the CVLM confirmed the correct targeting of this region in the sterotaxic experiments (Figure 7, E and F). Taken together, our results demonstrate that the CVLM GABAergic axons do not reach their target in absence of Vav3, suggesting that this GEF may be involved in the axon growth and/or guidance of these GABAergic inputs.

Vav3 Controls Axon Growth and Branching

Due to the fact that GABAergic VLM cells cannot be isolated and cultivated in vitro, we resorted to the use of GABAergic neurons from the hippocampus as a model to investigate the specific implication of Vav3 in axonal development. Vav3 is expressed endogenously in axons (Figure 8, A and B), growth cones (Figure 8, A and B), and tips of growth cone filopodia (Figure 8B) of hippocampal neurons, suggesting that this strategy may be an amenable way of investigating the role of this GEF in axon behavior. Using transient transfections, we observed that the overexpression of either full-length Vav3 or an N-terminally truncated, constitutively active Vav3 mutant protein in WT GABAergic neurons induces an increase and a reduction of maximal axon length and branch number, respectively (Figure 8, C and D). Using hippocampal cultures obtained from control and $Vav3^{-/-}$ mice, we also observed that the Vav3 deficiency led to an increase in the number of spontaneous axon branches in GABAergic cells (Figure 8, E and F) and to a reduction of growth cone areas (Figure 8, G and H). By contrast, it did not have any impact on the length of the longest axon (Figure 8, E and F), indicating that the positive effect induced by the constitutively active version of Vav3 in this response (see above, Figure 8D) is a *gain-of-function* effect or, alternatively, that a redundant Rho/Rac GEF can still ensure proper axon outgrowth when endogenous Vav3 is missing. Altogether, our results indicate that Vav3 is primarily required for normal axonal branching and growth cone formation, suggesting that retraction and/or inhibition of novo collateral extension is altered in absence of the GEF protein.

Vav family proteins have been associated with Eph receptor-dependent repulsion processes in mouse retinal ganglion cells. Such implication appears to be highly specific, because no defects have been observed in Semaphorin/plexin-dependent growth cone collapse in the same cell setting (Cowan *et al.*, 2005). To verify whether Vav3 could be involved in a similar pathway in GABAergic hippocampal neurons, we measured the growth cone collapse response of WT and Vav3-deficient hippocampal neurons upon stimulation with EphrinA1, a ligand for EphA family receptors. Vav3-deficient cells were less responsive than WT cells in this assay (Figure 8H, right panel). Taken together, these results indicate that Vav3 is important for the regulation of axon branching and growth cone morphology as well as for Ephrin-dependent axon collapsing responses in GABAergic cells.

DISCUSSION

In this work, we have shown that the cardiovascular defects found in Vav3-deficient mice are not caused by alterations in the intrinsic mechanoelastic and signaling properties of the
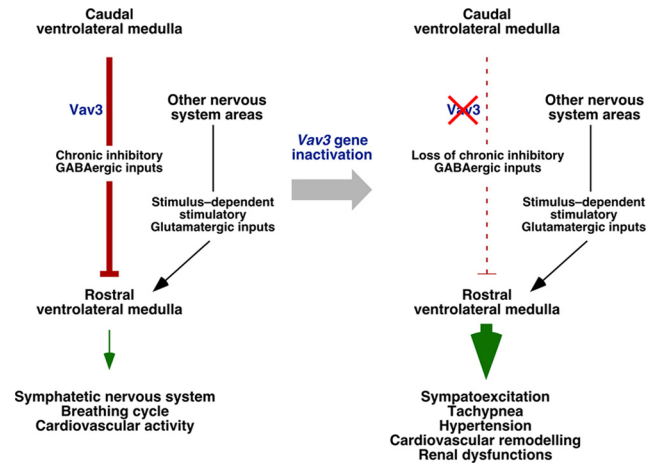

Figure 9. Summary of the results obtained in this work. Inhibitory and stimulatory actions are shown as blunted lines and arrows, respectively. Broken lines indicate disrupted axonal connections. Conditions present in WT and Vav3-deficient mice are shown in the left and right panel, respectively. See further details in main text.

vascular system or to tumorigenic processes in peripheral SNS areas such as the adrenal gland medulla. Consistent with the detection of tachycardia and chronic sympathoexcitation in those mice (Sauzeau *et al.*, 2006), our data indicate that the hypertension of $Vav3^{-/-}$ mice stems from a neurogenic defect probably located in the VLM. Using a combination of tract-tracing, immunohistochemical, and sterotaxic-based physiological experiments, we have shown that GABAergic neurons located in the CVLM of Vav3-deficient mice cannot reach efficiently their postsynaptic RVLM targets and that, consequently, the GABAergic transmission between the ventral and caudal parts of the VLM is impaired (Figure 9). Further support for the deregulated activity of this region in Vav3-deficient mice comes from the immunohistochemical data indicating the presence of hyperactivated sympathetic cells in their RVLMs and, in addition, by the observation that the plasma catecholamine levels drop to physiological concentrations in these animals when their defective GABAergic response is rescued by the microinjection of GABA receptor agonists in the RVLM. The GABAergic CVLM-RVLM connection represents a critical regulatory point to control sympathetic outflow from the VLM, because CVLM neurons feed tonic inhibitory signals to the RVLM and, at the same time, relay afferent signals derived from peripheral baroreceptors to that brainstem area (Guyenet, 2006). These two activities act coordinately to ensure the rapid restoration of normotensive values upon sporadic changes in blood pressure and, in addition, to reset the threshold for the activation of the baroreflex by RVLM cells, an action that in turn facilitates adaptative rises of blood pressure to new environmental, health or physiological conditions (Guyenet, 2006). Consistent with the role of VLM in the coordination of breathing activity via the adjacent Pre-Bötzinger complex, a brainstem area rostrally adjacent and overlapping to the RVLM (Bianchi *et al.*, 1995; Richter and Spyer, 2001), we have also observed that Vav3-deficient mice have alterations in the breathing activity that lead to chronic tachypnea (Figure 9).

Given that the nature and cytological complexity of the VLM is not compatible with mechanistic, cell biology-based experiments with cultured primary cells, we cannot discern at this moment the biological process impaired in $Vav3^{-/-}$ CVLM GABAergic cells. To bypass this hurdle, we have

used hippocampal GABAergic neurons as a model to obtain indirect information about the role of Vav3 in axon guidance-related processes. We have observed using this system that Vav3 is important for axonal arbor remodeling, for proper growth cone size, and for Ephrin/Eph receptor-mediated growth cone collapse responses, three critical steps that contribute to proper axon guidance that are under the control of Rho/Rac family proteins (Govek *et al.*, 2005). An implication of Vav3 and Vav2 in Ephrin-mediated growth cone collapse has been reported before in retina ganglion cells (Cowan *et al.*, 2005). This function is relevant for axon guidance, because $Vav2^{-/-};Vav3^{-/-}$-deficient mice show defects in ipsilateral retinogeniculate projections (Cowan *et al.*, 2005). However, unlike our case, this group has not found any defect in growth cone shape and axon branching in $Vav2^{-/-};Vav3^{-/-}$ retina ganglion cells (Cowan *et al.*, 2005). A plausible explanation for this discrepancy is that Vav3 may be required for normal growth cone shape only when neurons are cultured in poly-L-lysine alone, as previously described for other neuronal cultures (Chacon *et al.*, 2010). Alternatively, the neuron type used or the presence of other redundant Rho/Rac GEFs in retina ganglion cells may also explain this experimental discrepancy. Interestingly, it has been recently shown that *D. melanogaster* Vav protein also plays critical roles in axon guidance during late embryogenesis (Malartre *et al.*, 2010). The general implication of those Vav family members in general axon guidance processes in different neuronal subtypes suggest that Vav3 may also play similar functions in GABAergic VLM cells.

To date, the implication of the VLM in the long-term control of blood pressure has been based only in indirect short-term experiments carried out with fresh tissue sections or with anesthetized animals (Guyenet, 2006). Indeed, to our knowledge, the only clear link between the VLM and sustained blood pressure changes has been the observation that the adenoviral-mediated overexpression of endothelial nitric oxide synthase in the VLM induces transient bradycardia and low blood pressure levels in rats during a 5- to 10-d-long period postinfection (Kishi *et al.*, 2001; Kishi *et al.*, 2002), an effect attributed to an increase in GABA release induced by the local production of nitric oxide in this region (Kishi *et al.*, 2001). Our data complement these previous results by showing that the removal of GABAergic signaling leads to hypertension and, in addition, that the loss of blood normotensia can be sustained throughout the life of the investigated animals.

In summary, our results provide evidence for the implication of Vav3 in axon guidance events and in cardiorespiratory regulation, for the role of the VLM in long-term blood pressure control and, perhaps more importantly, suggest that some cases of neurogenic hypertension can derive from abnormal functioning of brain centers that feed tonic inhibitory signals into the RVLM. It would be important therefore revisiting the status of VLM regions in hypertension to verify whether alterations in that area may contribute to the origin of some neurogenic hypertension cases. Based on our data, hypertensive patients with associated tachycardia or with a previous history of borderline hypertension in their youth would be the best population groups to look at. The progressive and step-wise evolution of the sympathetic and cardiovascular dysfunctions developed in $Vav3^{-/-}$ mice also offers new possibilities for studying the evolution of additional SNS-dependent events and for dissecting in more detail the multiple synergistic cross-talk established by physiological circuits and tissues in cardiovascular disease.

REFERENCES

Bamji, S. X., Shimazu, K., Kimes, N., Huelsken, J., Birchmeier, W., Lu, B., and Reichardt, L. F. (2003). Role of beta-catenin in synaptic vehicle localization and presynaptic assembly. Neuron *13*, 719–731.

Bianchi, A. L., Denavit-Saubie, M., and Champagnat, J. (1995). Central control of breathing in mammals: neuronal circuitry, membrane properties, and neurotransmitters. Physiol. Rev. *75*, 1–45.

Blessing, W. W. (1988). Depressor neurons in rabbit caudal medulla act via GABA receptors in rostral medulla. Am J. Physiol. *254*, H686–H692.

Bustelo, X. R. (2000). Regulatory and signaling properties of the Vav family. Mol. Cell. Biol. *20*, 1461–1477.

Bustelo, X. R. (2001). Vav proteins, adaptors and cell signaling. Oncogene *20*, 6372–6381.

Bustelo, X. R., and Couceiro, J. R. (2008). Vav3. UCSD Nature Mol Pages, (DOI: 10.1038/mp.a002362.002301).

Cella, M., Fujikawa, K., Tassi, I., Kim, S., Latinis, K., Nishi, S., Yokoyama, W., Colonna, M., and Swat, W. (2004). Differential requirements for Vav proteins in DAP10- and ITAM-mediated NK cell cytotoxicity. J. Exper. Med. *200*, 817–823.

Chacon, M. R., Fernandez, G., and Rico, B. (2010). Focal adhesion kinase functions downstream of Sema3A signaling during axonal remodeling. Mol. Cell. Neurosci. *44*, 30–42.

Cowan, C. W., Shao, Y. R., Sahin, M., Shamah, S. M., Lin, M. Z., Greer, P. L., Gao, S., Griffith, E. C., Brugge, J. S., and Greenberg, M. E. (2005). Vav family GEFs link activated Ephs to endocytosis and axon guidance. Neuron *46*, 205–217.

Faccio, R., Teitelbaum, S. L., Fujikawa, K., Chappel, J., Zallone, A., Tybulewicz, V. L., Ross, F. P., and Swat, W. (2005). Vav3 regulates osteoclast function and bone mass. Nat. Med. *11*, 284–290.

Frankin, B. J., and Paxinos, G. T. (1996). The Mouse brain in stereotaxic coordinates. New York: Academic Press.

Fujikawa, K., Miletic, A. V., Alt, F. W., Faccio, R., Brown, T., Hoog, J., Fredericks, J., Nishi, S., Mildiner, S., Moores, S. L., Brugge, J., Rosen, F. S., and Swat, W. (2003). Vav1/2/3-null mice define an essential role for Vav family proteins in lymphocyte development and activation but a differential requirement in MAPK signaling in T and B cells. J. Exper. Med. *198*, 1595–1608.

Gakidis, M. A., Cullere, X., Olson, T., Wilsbacher, J. L., Zhang, B., Moores, S. L., Ley, K., Swat, W., Mayadas, T., and Brugge, J. S. (2004). Vav GEFs are required for beta2 integrin-dependent functions of neutrophils. J. Cell Biol. *166*, 273–282.

Govek, E. E., Newey, S. E., and Van Aelst, L. (2005). The role of the Rho GTPases in neuronal development. Genes Dev. *19*, 1–49.

Guyenet, P. G. (2006). The sympathetic control of blood pressure. Nat. Rev. Neurosci. *7*, 335–346.

Hall, A. B., Gakidis, M. A., Glogauer, M., Wilsbacher, J. L., Gao, S., Swat, W., and Brugge, J. S. (2006). Requirements for Vav guanine nucleotide exchange factors and Rho GTPases in FcgammaR- and complement-mediated phagocytosis. Immunity *24*, 305–316.

Hunter, S. G., Zhuang, G., Brantley-Sieders, D., Swat, W., Cowan, C. W., and Chen, J. (2006). Essential role of Vav family guanine nucleotide exchange factors in EphA receptor-mediated angiogenesis. Mol. Cell. Biol. *26*, 4830–4842.

Julius, S., and Nesbitt, S. (1996). Sympathetic overactivity in hypertension: a moving target. Am J. Hypertens *9*, 113S–120S.

Kishi, T., Hirooka, Y., Ito, K., Sakai, K., Shimokawa, H., and Takeshita, A. (2002). Cardiovascular effects of overexpression of endothelial nitric oxide synthase in the rostral ventrolateral medulla in stroke-prone spontaneously hypertensive rats. Hypertension *39*, 264–268.

Kishi, T., Hirooka, Y., Sakai, K., Shigematsu, H., Shimokawa, H., and Takeshita, A. (2001). Overexpression of eNOS in the RVLM causes hypotension and bradycardia via GABA release. Hypertension *38*, 896–901.

Lenders, J. W., Eisenhofer, G., Mannelli, M., and Pacak, K. (2005). Phaeochromocytoma. Lancet *366*, 665–675.

Li, Y. W., Gieroba, Z. J., McAllen, R. M., and Blessing, W. W. (1991). Neurons in rabbit caudal ventrolateral medulla inhibit bulbospinal barosensitive neurons in rostral medulla. Am. J. Physiol. *261*, R44–51.

Malartre, M., Ayaz, D., Amador, F. F., and Martin-Bermudo, M. D. (2010). The guanine exchange factor vav controls axon growth and guidance during Drosophila development. J. Neurosci. *30*, 2257–2267.

Masuda, N., Terui, N., Koshiya, N., and Kumada, M. (1991). Neurons in the caudal ventrolateral medulla mediate the arterial baroreceptor reflex by inhibiting barosensitive reticulospinal neurons in the rostral ventrolateral medulla in rabbits. J. Auton Nerv. Syst. *34*, 103–117.

Miletic, A. V., Graham, D. B., Montgrain, V., Fujikawa, K., Kloeppel, T., Brim, K., Weaver, B., Schreiber, R., Xavier, R., and Swat, W. (2007). Vav proteins control MyD88-dependent oxidative burst. Blood *109*, 3360–3368.

Movilla, N., and Bustelo, X. R. (1999). Biological and regulatory properties of Vav-3, a new member of the Vav family of oncoproteins. Mol. Cell. Biol. *19*, 7870–7885.

Pearce, A. C., McCarty, O. J., Calaminus, S. D., Vigorito, E., Turner, M., and Watson, S. P. (2007). Vav family proteins are required for optimal regulation of PLCgamma2 by integrin alphaIIbbeta3. Biochem. J. *401*, 753–761.

Pearce, A. C., Senis, Y. A., Billadeau, D. D., Turner, M., Watson, S. P., and Vigorito, E. (2004). Vav1 and vav3 have critical but redundant roles in mediating platelet activation by collagen. J. Biol. Chem. *279*, 53955–53962.

Quevedo, C., Sauzeau, V., Menacho-Marquez, M., Castro-Castro, A., and Bustelo, X. R. (2010). Vav3-deficient mice exhibit a transient delay in cerebellar development. Mol. Biol. Cell *21*, 1125–1139.

Reiner, A., Veenman, C. L., Medina, L., Jiao, Y., Del Mar, N., and Honig, M. G. (2000). Pathway tracing using biotinylated dextran amines. J. Neurosci. Methods *103*, 23–37.

Richter, D. W., and Spyer, K. M. (2001). Studying rhythmogenesis of breathing: comparison of in vivo and in vitro models. Trends Neurosci. *24*, 464–472.

Rico, B., Beggs, H. E., Schahin-Reed, D., Kimes, N., Schmidt, A., and Reichardt, L. F. (2004). Nat. Neurosci. *7*, 1059–1069.

Sauzeau, V., Jerkic, M., Lopez-Novoa, J. M., and Bustelo, X. R. (2007). Loss of Vav2 proto-oncogene causes tachycardia and cardiovascular disease in mice. Mol. Biol. Cell *18*, 943–952.

Sauzeau, V., Sevilla, M. A., Montro, M. J., and Bustelo, X. R. (2010). The Rho/Rac exchange factor Vav2 controls nitric oxide-dependent responses in vascular smooth muscle cells. J. Clin Invest. *120*, 315–330.

Sauzeau, V., Sevilla, M. A., Rivas-Elena, J. V., de Alava, E., Montero, M. J., Lopez-Novoa, J. M., and Bustelo, X. R. (2006). Vav3 proto-oncogene deficiency leads to sympathetic hyperactivity and cardiovascular dysfunction. Nat. Med. *12*, 841–845.

Saveliev, A., Vanes, L., Ksionda, O., Rapley, J., Smerdon, S. J., Rittinger, K., and Tybulewicz, V. L. (2009). Function of the nucleotide exchange activity of vav1 in T cell development and activation. Sci. Signal. *2*, ra83.

Schreihofer, A. M., and Guyenet, P. G. (2003). Baro-activated neurons with pulse-modulated activity in the rat caudal ventrolateral medulla express GAD67 mRNA. J. Neurophysiol. *89*, 1265–1277.

Schuhmacher, A. J., Guerra, C., Sauzeau, V., Canamero, M., Bustelo, X. R., and Barbacid, M. (2008). A mouse model for Costello syndrome reveals an Ang II-mediated hypertensive condition. J. Clin. Invest. *118*, 2169–2179.

Thrasher, T. N. (2005). Baroreceptors, baroreceptor unloading, and the long-term control of blood pressure. Am J. Physiol. Regul. Integr. Comp. Physiol. *288*, R819–R827.

Tolentino-Silva, F. P., Haxhiu, M. A., Ernsberger, P., Waldbaum, S., and Dreshaj, I. A. (2000). Differential cardiorespiratory control elicited by activation of ventral medullary sites in mice. J. Appl. Physiol. *89*, 437–444.

Turner, M., and Billadeau, D. D. (2002). VAV proteins as signal integrators for multi-subunit immune-recognition receptors. Nat. Rev. Immunol. *2*, 476–486.

Yoshida, S., Matsubara, T., Uemura, A., Iguchi, A., and Hotta, N. (2002). Role of medial amygdala in controlling hemodynamics via GABA(A) receptor in anesthetized rats. Circ. J. *66*, 197–203.